Process-based upscaling of reactive flow in geological formations

Meulenbroek, Bernard; Farajzadeh, Rouhi; Bruining, Hans

DOI
10.1016/j.ijheatmasstransfer.2020.119969

Publication date
2020

Document Version
Final published version

Published in
International Journal of Heat and Mass Transfer

International Journal of Heat and Mass Transfer 157 (2020) 119969

Contents lists available at ScienceDirect

International Journal of Heat and Mass Transfer

journal homepage: www.elsevier.com/locate/hmt

Process-based upscaling of reactive flow in geological formations

Bernard Meulenbroek[a,*], Rouhi Farajzadeh[b], Hans Bruining[b]

[a] Delft University of Technology, Delft Institute of Applied Mathematics, Mekelweg 4, 2628 CD, Delft, The Netherlands
[b] Delft University of Technology, Department of GeoScience and Engineering, Stevinweg 1, 2628 CN, Delft, The Netherlands

ARTICLE INFO

Article history:
Received 17 July 2019
Revised 30 April 2020
Accepted 16 May 2020
Available online 18 June 2020

Keywords:
Reactive flow modeling
Peclet/Damkohler number phasespace
Reservoir conditions
Temperature/pH/salinity dependence

ABSTRACT

Recently, there is an increased interest in reactive flow in porous media, in groundwater, agricultural and fuel recovery applications. Reactive flow modeling involves vastly different reaction rates, i.e., differing by many orders of magnitude. Solving the ensuing model equations can be computationally intensive. Categorizing reactions according to their speeds makes it possible to greatly simplify the relevant model equations. Indeed some reactions proceed so slow that they can be disregarded. Other reactions occur so fast that they are well described by thermodynamic equilibrium in the time and spatial region of interest. At intermediate rates kinetics needs to be taken into account. In this paper, we categorize selected reactions as slow, fast or intermediate. We model 2D radially symmetric reactive flow with a reaction-convection-diffusion equation. We show that we can subdivide the $PeDa_{II}$ phasespace in three regions. Region I (slow reaction); reaction can be ignored, region II (intermediate reaction); initially kinetics need to be taken into account, region III (fast reaction); all reaction takes places in a very narrow region around the injection point. We investigate these aspects for a few specific examples. We compute the location in phase space of a few selected minerals depending on salinity and temperature. We note that the conditions, e.g., salinity and temperature may be essential for assigning the reaction to the correct region in phase space. The methodology described can be applied to any mineral precipitation/decomposition problem and consequently greatly simplifies reactive flow modeling in porous media.

1. Introduction

The efficiency of improved or enhanced oil recovery (IOR/EOR) processes is often influenced by the composition of the flowing aqueous phase and is thus affected by the mass exchange between fluid and solid phases [1]. For example, the rheology of water-soluble polymers or the magnitude of the interfacial-tension reduction by surfactants strongly depends on the ionic strength and hardness (concentration of divalent cations) of the aqueous phase and strongly influence the displacement efficiency [2]. In recent years, the additional oil extracted by tuning the composition of the injected water has led to more detailed investigation of the nature of the interactions between the rock and the fluids residing in the pore [3].

Additionally, dissolution and precipitation of minerals have a considerable effect on the permeability of the reservoir [4]. The permeability impairment can lead to high circulation costs and loss of injectivity [5]. Permeability impairment occurs both due to particle release and subsequent retention [5] and precipitation of minerals [4].

When a fluid is injected into an oil reservoir, the chemical species in the solution will interact with the species in the reservoir fluids contained in the pores and/or the substances on the rock grains. As these species are subject to transport in the reservoir, in the numerical modelling of the process it is essential to know the final composition of the solution at the end of each timestep [6–8]. This is determined by how far the reactions are completed within each grid cell during each timestep [7,8]. For fast reactions, the front develops over a short distance, while for slow reactions fronts develop over a longer distance from the injection point.

Subsurface formations are composed of several minerals, which adds another complexity in modelling of geochemical reactions [9,10]. The time required to reach equilibrium can vary from seconds to (a few thousand) years for different minerals [11,12]. Therefore, in the numerical simulations, during a single time step, the concentration of some species could be over- or under-estimated. There are two important methods in geo-chemical modelling, viz., the Local Equilibrium Approach (LEA) and the Kinetic Approach (KA) [13]. The LEA, which is the most common ap-

* Corresponding author.
E-mail address: b.j.meulenbroek@tudelft.nl (B. Meulenbroek).

https://doi.org/10.1016/j.ijheatmasstransfer.2020.119969

proach in reactive transport modelling, assumes that the reactions take place instantaneously and neglects the duration of the reaction. This approach is preferred because of its simplicity and the fact that it is computationally less expensive. However, the local equilibrium approach may over- or underestimate the concentration of the species in the solution, e.g., due to heterogeneity [14–16].

Indeed, the reactions in nature do not always reach equilibrium within the time and space of interest. The Kinetic Approach describes the time-dependency of the reactions. Some reactions complete faster than others and therefore the assumption of local equilibrium does not hold in some practical cases. For example, in IOR/EOR applications, the injected fluid (which might be in equilibrium itself) is usually out of equilibrium with the rock (this is referred to as partial equilibrium)[1]. The reservoir rocks consist of several components whose reactions with the injected fluid have different rates. Therefore, the kinetics of the reactions in this case determines the composition of the fluid (and consequently the efficiency of the injected chemical). This poses challenges when the results of the lab-scale experiments are translated to large-scale field applications, because different time and length scales are involved. For this purpose, when the experiments are modelled, special attention should be given to correctly calculate the equilibrium time (T_{eq}) and the equilibrium distance (R_{eq}) of the relevant minerals. These quantities are used as guidelines for selection of the temporal and spatial resolution of the numerical simulations.

It is difficult (if not impossible) to develop a general upscaling technique to account for the geochemical reactions in different IOR/EOR processes. Apart from the geological uncertainties and the intrinsic heterogeneity of the formations, the information on the mineralogical composition of the rocks is scarce. Even if the mineralogy of the formation is partially known, the surface area available for the reactions is hard to measure. Notably, the bulk mineralogical composition determined from X-Ray Diffraction (XRD) data can significantly differ from the surface composition obtained by X-Ray Photoelectron Spectroscopic (XPS) [17].

Therefore, it is suggested to follow a simpler approach, which is process specific. In such an approach, only relevant minerals affecting the efficiency of the process are listed. The main minerals considered are Na (K, Ca) - silicate (carbonate) minerals (see [9–12] for weathering rates). The particular interest is then to evaluate the time and distance that is required for the injected fluid to reach the equilibrium state. The equilibrium time (T_{eq}) and the equilibrium distance (R_{eq}) are indications of the temporal and spatial resolutions of the simulations.

It is therefore our objective to include mineral reactions in the modeling of reactive flow in porous media. This problem can be studied on two characteristic length scales R_{char}: the well radius and the reservoir size. This choice defines also a characteristic time T_{char}, see Section 2.3. This gives the opportunity to study the equilibrium length (R_{eq}) and equilibrium time (T_{eq}) of these reactions with respect to the characteristic length and time. We distinguish three possibilities (I) $R_{eq} \gg R_{char}$, the whole reservoir will be at the injection concentration (II) $R_{eq} \ll R_{char}$, the reservoir will be at the initial concentration and (III) $R_{eq} \sim R_{char}$, the concentration is varying throughout the whole reservoir. Note that in cases (I) and (II) the reservoir can be considered at equilibrium and kinetics do not have to be taken into account.

The paper is organized as follows. Section 2 gives the physical model and model equations. In Section 2.6 the model equations are reduced to a second order ODE with boundary conditions. Section 3 shows and compares analytical results for different values of the physical parameters. Section 4 computes R_{eq}, and we determine whether we are in case (I, II, III) for a given set of minerals. We end the paper with some conclusions in Section 5.

2. Physical and mathematical model

In this section we will present single phase transport and reaction (dissolution and precipitation of the omni-present minerals), using a reaction convection diffusion model. In the model equations we will use capital letters for dimensional variables, variables with subscript c for characteristic scales and small letters for dimensionless variables.

2.1. Reaction rates

The methodology presented in this work can be applied to general dissolution/precipitation reactions. As illustration we consider the following explicit reactions:

K- feldspar: $KAlSi_3O_8 + 4\,H_2O + 4\,H^+ \leftrightarrow Al^{3+} + 3\,H_4SiO_4 + K^+$
Kaolinite: $Al_2Si_2O_5(OH)_4 + 6\,H^+ \leftrightarrow H_2O + 2\,H_4SiO_4 + 2\,Al^{3+}$
Anhydrite: $CaSO_4 \leftrightarrow Ca^{2+} + SO_4^{2-}$
Calcite : $CaCO_3 \leftrightarrow Ca^{2+} + CO_3^{2-}$

For the reaction rates S_1 we apply the often adopted simplifying assumption (see, however, [18]) of using the law of mass action and obtain (see [10])

$$S_1 = \kappa\,(A_1/V)(1 - \frac{IAP}{K})^n, \tag{1}$$

where IAP is the ionic activity product, K is the equilibrium constant, $\frac{A_1}{V}$ $[m^2/m^3]$ is the reactive surface area per cubic meter water; κ $[mol/(m^2\ s)]$ is a temperature dependent rate constant. In practice the value of n is chosen to mimic experimentally determined reaction rates, and here chosen to be equal to one. The rate constant can be considered in its Arrhenius form

$$\kappa = k_{10} e^{-E_a/(RT)}, \tag{2}$$

where k_{10} is the frequency factor, E_a is the activation energy, R is the gas constant and T is temperature in K.

As concentration of interest, C, we use the dissolved ions, (e.g., Al^{3+}) or dissolved molecules (e.g. H_4SiO_4). Moreover we assume that the reactions occur independent of each other and that we can single out one specific ion or molecule. This approach cannot describe the decomposition of the mineral, but does allow to classify reactions into slow, intermediate and fast reactions.

We assume furthermore isothermal flow at constant pH, which means that we assume that the ion activity product is related to the dissolved mineral concentration C, "independent" of other concentrations, which are present in excess so that they can be assumed to be constant. Various temperatures and pH values can be considered. Given its approximate nature it is not warranted to assume non-linear dependences, and we assume that IAP is proportional to C, i.e.,

$$IAP \sim C. \tag{3}$$

We note that similar simplifying assumptions are made in the literature (see [7]). We then lump the proportionality constant and K together into the constant C_0 and obtain

$$S_1 = \kappa \frac{A_1}{V}\left(1 - \frac{C}{C_0}\right). \tag{4}$$

Setting $A = \frac{A_1}{\rho_w V}$ we have reactive surface in m^2/kg-water and $S = \frac{S_1}{\rho_w}$ we obtain the reaction rate in [mol/kg-water / s] and we finally obtain

$$S = A\kappa\left(1 - \frac{C}{C_0}\right). \tag{5}$$

2.2. Transport equations

We assume incompressible flow, which means that we have the following equation for the interstitial velocity $\mathbf{V}$

$$\nabla \cdot \mathbf{V} = 0. \tag{6}$$

Transport is described with a reaction convection diffusion equation

$$\frac{\partial C}{\partial T} + \nabla \cdot (C\mathbf{V}) = D\Delta C + S, \tag{7}$$

where the reaction rate S is given in Section 2.1. The concentration initially present in the reservoir is denoted by C_0 [mol / (kg-water)]; we assume that the reservoir initially is in equilibrium, meaning that we disregard slow naturally occurring variations that take place after times longer than our timeframe of interest. This means that, from a practical point of view, the reservoir is initially at the equilibrium concentration (at the initially present environmental conditions). This means that reaction will take place if we perturb the initial concentration C_0 to C.

We are looking for radially symmetric solutions $\mathbf{V} = V(r,t)\hat{\mathbf{r}}$, $C = C(r,t)$, which means that equation (6) reduces to

$$\frac{1}{R}\frac{\partial}{\partial R}(RV) = 0 \tag{8}$$

and equations (7)-(5) yield

$$\frac{\partial C}{\partial T} + \frac{1}{R}\frac{\partial}{\partial R}(RCV) = D\frac{1}{R}\frac{\partial}{\partial R}\left(R\frac{\partial C}{\partial R}\right) + A\kappa\left(1 - \frac{C}{C_0}\right), \tag{9}$$

which reduces to

$$\frac{\partial C}{\partial T} + V\frac{\partial C}{\partial R} = D\frac{1}{R}\frac{\partial}{\partial R}\left(R\frac{\partial C}{\partial R}\right) + A\kappa\left(1 - \frac{C}{C_0}\right) \tag{10}$$

because

$$\frac{\partial}{\partial R}(RCV) = RV\frac{\partial C}{\partial R} + C\frac{\partial RV}{\partial R} = RV\frac{\partial C}{\partial R} \tag{11}$$

due to equation (8).

Equations (8) and (10) are made dimensionless using the characteristic length R_c, characteristic time T_c (discussed below) and the initial equilibrium concentration C_0 as follows:

$$r = \frac{R}{R_c},\ T = \frac{T}{T_c} \Rightarrow v = V\cdot\frac{T_c}{R_c} \tag{12}$$

$$c = \frac{C - C_0}{C_0}, \tag{13}$$

i.e., $c = 0$ corresponds to the equilibrium concentration. Equation (8) reads in dimensionless form

$$\frac{1}{r}\frac{\partial}{\partial r}(rv) = 0 \Rightarrow \frac{\partial}{\partial r}(rv) = 0 \tag{14}$$

and equation (10) reads

$$\frac{\partial c}{\partial t} + v\frac{\partial c}{\partial r} = \frac{1}{Pe}\frac{1}{r}\frac{\partial}{\partial r}\left(r\frac{\partial c}{\partial r}\right) - Da_I c, \tag{15}$$

where we used the Peclet number

$$Pe = \frac{R_c^2}{DT_c} = \frac{V_c R_c}{D}, \tag{16}$$

which denotes the ratio between convection and diffusion. We also used the first Damkohler number

$$Da_I = \frac{A\kappa T_c}{C_0} = \frac{A\kappa R_c}{C_0 V_c}, \tag{17}$$

which denotes the ratio between reaction and convection. Furthermore we will also use the Damkohler number II

$$Da_{II} = PeDa_I = \frac{A\kappa R_c^2}{C_0 D}, \tag{18}$$

which denotes the ratio between reaction and diffusion.

2.3. Discussion of the scales

Two scales have to be chosen: the characteristic length R_c and a characteristic interstitial velocity V_c (or a characteristic time T_c).We are mainly interested in clogging around the inlet, which means that we will set $R_c = R_w$ (well radius) in our computations for the field scale. For reasons of flexibility we will maintain a general R_c, to allow other choices, like $R_c = R_{res}$ (reservoir radius).

Solving equations (14) yields $v = \frac{K_1}{r}$ (where K_1 is a constant), which is in dimensional form

$$V = V_c R_c \frac{K_1}{R};$$

this means that V varies throughout the reservoir and multiple reasonable choices for V_c can be made. However, choosing the character velocity as the velocity at R_w, i.e., $V_c = V(R_w)$ implies that the constant $K_1 = 1$ which simplifies our expressions; in this work we will make this choice.

Using the characteristic velocity V_c and the characteristic length R_c we have the characteristic time

$$T_c = \frac{R_c}{V_c}. \tag{19}$$

Note that the characteristic time depends on whether we choose the reservoir radius or the well radius as our characteristic length.

In Section 4 we will discuss the behaviour of four minerals (anhydrite, calcite, kaolinite, K-feldspar) under two conditions (low salinity and alkaline flood) both at low injection velocity/low Pe (named "field") and higher injection velocity/higher Pe (named "experiment"). The field and experimental parameters are given in Tables 2 and 3; the parameters concerning the four minerals are given in Table 4.

2.4. Summary of the mathematical model

The governing equations are

$$\frac{\partial}{\partial r}(rv) = 0 \tag{20}$$

and

$$\frac{\partial c}{\partial t} + v\frac{\partial c}{\partial r} = \frac{1}{Pe}\frac{1}{r}\frac{\partial}{\partial r}\left(r\frac{\partial c}{\partial r}\right) - Da_I c. \tag{21}$$

We inject a solution at concentration $C = C_{inj} \neq C_0$ at a constant injection velocity at $r = r_w$, i.e.,

$$V = V_c\frac{R_c}{R_w} \text{ at } r = r_w, \tag{22}$$

i.e.,

$$v = \frac{1}{r_w} \text{ at } r = r_w, \tag{23}$$

This means that we have a Danckwerts boundary condition for the concentration at the well $r = r_w\frac{R_w}{R_c}$ (note that rv is constant due to equation (20))

$$(rv)c - \frac{1}{Pe}\cdot\left(r\frac{\partial c}{\partial r}\right) = (rv)c^\star \text{ at } r = r_w, \tag{24}$$

where $c^\star$ is the dimensionless injection concentration

$$c^\star = \frac{C_{inj} - C_0}{C_0}. \tag{25}$$

For large values of Pe, the boundary condition (24) can be approximated by

$$c \approx c^\star \text{ at } r = r_w, \tag{26}$$

Table 1
Nomenclature; capital letters are used to denote dimensional variables, small letters are used to denote the corresponding dimensionless variables.

variable	description	unit	subscript	
A	reactive surface area	m^2/(kg-water)	$_0$	initial
C	concentration	mol/(kg-water)	$_{inj}$	injection
D	diffusion coefficient	m^2/s	$_{ss}$	steady state
Da_I	Damkohler number I (see Eq. 17)	-	$_{tr}$	transient
Da_{II}	Damkohler number II (see Eq. 18)	-		
Pe	Peclet number (see Eq. 16)	-	$_w$	well
R	(radial) distance	m	$_{res}$	reservoir
S	reaction rate (Eq. 5)	[mol / (kg-water s)]		
T	time	[s]	$_c$	characteristic
$\mathbf{V}$	velocity	m/s		
κ	rate constant	mol/(m^2s)		

Table 2
Parameters and scales (field).

well radius	R_w	10^{-1} [m]
reservoir radius	R_{res}	10^3 [m]
characteristic length	R_c	10^{-1} [m]
characteristic velocity	V_c	10^{-6} [m/s]
diffusion coefficient	D	10^{-9} [m^2/s]
Peclet number	Pe	100

Table 3
Parameters and scales (experimental).

characteristic length	R_c	10^{-1} [m]
characteristic velocity	V_c	$5 \cdot 10^{-5}$ [m/s]
diffusion coefficient	D	10^{-9} [m^2/s]
Peclet number	Pe	5000

which means that in this case the concentration is approximately the injection concentration at $r = r_w$. At $r = r_{res}$ we have

$$\frac{\partial c}{\partial r} = 0, \tag{27}$$

and at $t = 0$ we have the initial condition

$$c = 0 \text{ at } t = 0. \tag{28}$$

The dimensionless parameters Pe and Da_I are given by

$$Pe = \frac{R_c V_c}{D}, \; Da_I = \frac{A\kappa R_c}{C_0 V_c}. \tag{29}$$

Note that Pe is independent of the length scale chosen (because we chose $V_c = V_(R_w)$ and $V \sim \frac{1}{R}$), but that both Da_I and $Da_{II} = Da_I Pe$ depend on the length scale.

2.5. Final note on the length scale

Besides that the Da_I depends on the length scale, the location of the boundary conditions depends on this choice as well. This changes the nature of the solutions of our problem.

If we use $R_c = R_w$ as our characteristic length scale, our boundary conditions are at

$$r = \frac{R_w}{R_w} = 1 \text{ and } r = \frac{R_{res}}{R_w} \approx \infty, \tag{30}$$

whereas if we take $R_c = R_{res}$ as our characteristic length scale we have our boundary conditions at

$$r = \frac{R_w}{R_{res}} \approx 0 \text{ and } r = \frac{R_{res}}{R_{res}} = 1. \tag{31}$$

This means that because the functional form of the solution will change - the problems at these two length scales should be treated separately. In this work we will focus on the $R_c = R_w$ choice.

2.6. Analytical steady-state solution and transients

In this section we will solve our problem (20)-(28) on the characteristic scale $R_c = R_w$.

The solution of the velocity profile is straightforward

$$\frac{\partial}{\partial r}(rv) = 0, \; v(1) = 1 \Rightarrow v = \frac{1}{r}. \tag{32}$$

The solution of problem (20)-(28) is the superposition of a time independent steady state profile and a transient profile, i.e.,

$$c(r,t) = c_{ss}(r) + c_{tr}(r,t), \tag{33}$$

where the steady state satisfies a second order ODE

$$\frac{dc_{ss}}{dr} = \frac{1}{Pe}\frac{d}{dr}\left(r\frac{dc_{ss}}{dr}\right) - Da_1 r c_{ss}, \tag{34}$$

which can be rewritten as

$$\frac{d^2 c_{ss}}{dr^2} = \frac{(Pe-1)}{r}\frac{dc_{ss}}{dr} + Da_1 Pe c_{ss}. \tag{35}$$

The boundary conditions (24)-(27) yield

$$c_{ss} - \frac{r}{Pe}\frac{dc_{ss}}{dr} = c^\star \text{ at } r = 1 \text{ and } \frac{dc_{ss}}{dr} = 0 \text{ as } r \to \infty. \tag{36}$$

Table 4
Mineral parameters low sal. Alaska at 60C (field and experimental) and Alkali field, see [19]. The Damkohler numbers are calculated using equation (18) and Tables 2 and 3 .

mineral	A [m^2/kgw]	κ [mol/(m^2s)]	C_0 [mol/kgw]	Da_{II}
Anhydrite (low sal.)	40	$1.2 \cdot 10^{-3}$	$1.74 \cdot 10^{-2}$	$2.7 \cdot 10^{7}$
(alkaline)	40	$1.2 \cdot 10^{-3}$	$4.7 \cdot 10^{-2}$	$1.0 \cdot 10^{7}$
Calcite (low sal.)	40	$4.2 \cdot 10^{-6}$	$2.63 \cdot 10^{-3}$	$6 \cdot 10^{5}$
(alkaline)	40	$4.2 \cdot 10^{-6}$	$9.4 \cdot 10^{-6}$	$2 \cdot 10^{8}$
Kaolinite (low sal.)	40	$1.9 \cdot 10^{-17}$	$3.8 \cdot 10^{-6}$	$2 \cdot 10^{-3}$
(alkaline)	40	$1.9 \cdot 10^{-17}$	$1.2 \cdot 10^{-3}$	$4.7 \cdot 10^{-6}$
K-Feldspar (low sal.)	40	$3.11 \cdot 10^{-20}$	$1.29 \cdot 10^{-4}$	$1.1 \cdot 10^{-7}$
(alkaline)	40	$3.11 \cdot 10^{-20}$	$7 \cdot 10^{-4}$	$2.2 \cdot 10^{-9}$

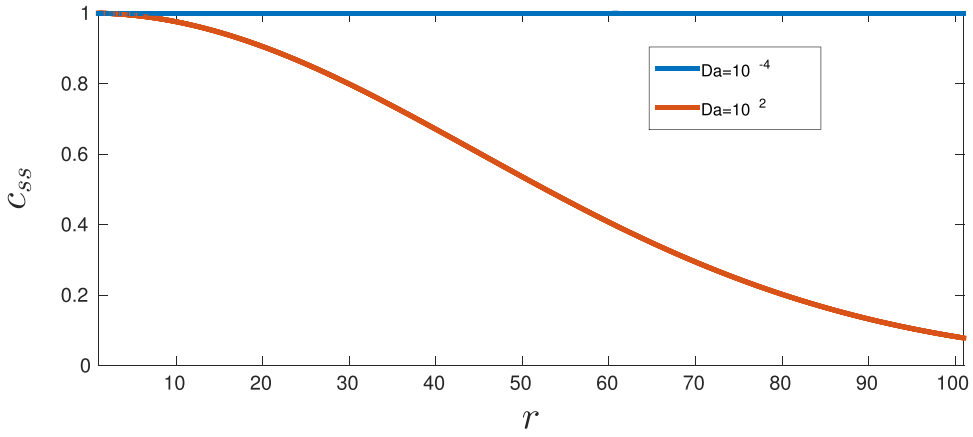

Fig. 1. Steady state concentration profile c_{ss} as function of r (Regime A) for a fixed value of $Pe = 10^5$ and two values of Da_{II}; $Da_{II} = 10^{-4}$ and $Da_{II} = 10^2$.

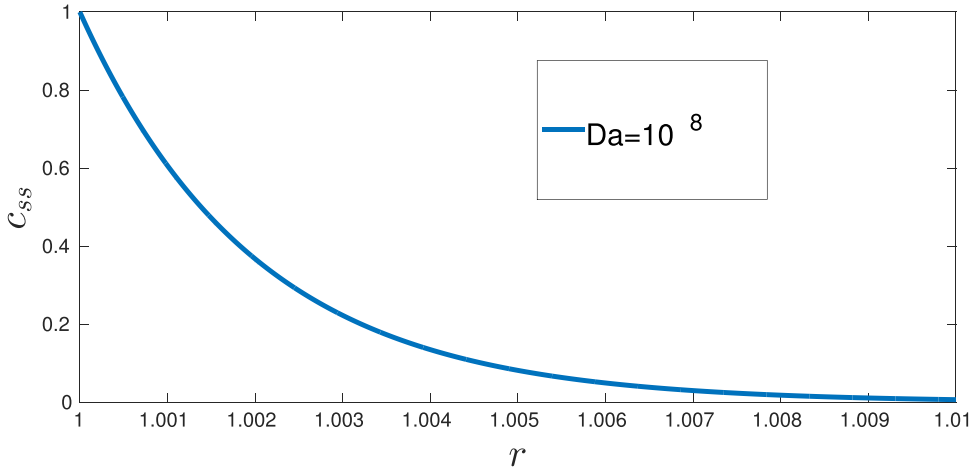

Fig. 2. Steady state concentration profile c_{ss} as function of r (Regime A) for a fixed value of $Pe = 10^5$ and $Da_{II} = 10^8$. Note the different scale on the r-axis compared to Fig. 1 .

For the transients we need to solve the initial value problem

$$r\frac{\partial c_{tr}}{\partial t} + \frac{\partial c_{tr}}{\partial r} = \frac{1}{Pe}\frac{\partial}{\partial r}\left(r\frac{\partial c_{tr}}{\partial r}\right) - Da_1 r c_{tr} \tag{37}$$

with boundary conditions

$$c_{tr} - \frac{r}{Pe}\frac{dc_{tr}}{dr} = 0 \text{ at } r = 1 \text{ and } \frac{dc_{tr}}{dr} = 0 \text{ as } r \to \infty. \tag{38}$$

and initial condition

$$c_{tr}(r, 0) = -c_{ss}(r). \tag{39}$$

The solution of the steady state problem is already sufficient to answer our research question; computation of the transients is not necessary in this paper.

3. Analytical steady-state solutions of the model equations

Equations (35) -(36) determine $c_{ss}(r)$ for all values of Pe and Da_{II}. Finding the complete explicit solution however is difficult due the large variation in the values of the Pe and Da_{II}. We will subdivide the $PeDa_{II}-$ parameter space in three regimes and for each of the three regimes we will determine (an approximation to) $c_{ss}(r)$ using a different method.

Regime A $Da_{II} \ll Pe^2$, assumption A: $c_{ss}(r) \approx c_{ss,A}(r)$
Regime B $Da_{II} \sim Pe^2$, assumption B: $c_{ss}(r) \approx c_{ss,B}(r)$
Regime C $Da_{II} \gg Pe^2$, assumption C: $c_{ss}(r) \approx c_{ss,C}(r)$

Note that the assumption depends on the regime, i.e., we will have a different functional form of the approximation for each regime. The solution for Regime A is given in Section 3.1, the solution for Regime B is given in Section 3.2 and the solution for Regime C is given in Section 3.3. We then merge these results and discuss the full $PeDa_{II}$-phasespace in Section 3.4, using the appropriate approximations (A,B,C) for c_{ss} in each point of the phasespace.

3.1. Regime a: $\mathrm{Da_{II}} \ll \mathrm{Pe}^2$

In Regime A the diffusion term $\frac{d^2 c_{ss}}{dr^2}$ can be neglected and equations (35)-(36) can now be simplified and solved (see Appendix A.1 for details) and the final result is as follows

$$c_{ss} = c^\star e^{-\alpha(r^2-1)}, \ \alpha = \frac{Da_{II}}{2(Pe-1)}. \tag{40}$$

In Figs. 1 and 2 we plot $c_{ss}(r)$ for a fixed $Pe = 10^5$ and three different Da_{II} numbers; $Da_{II} = 10^{-4}$, $Da_{II} = 10^2$ and $Da_{II} = 10^8$. We observe three types of behaviour; for small Da_{II} the whole reservoir is almost at the injection concentration, see the upper curve in Fig. 1. for high Da_{II} the whole reservoir remains at initial concentration, see Fig. 2 and note the different scales on the r-axis. For intermediate Da_{II} we observe mixed behaviour, see the lower curve in Fig. 1. We will discuss this in more detail in Section 4.

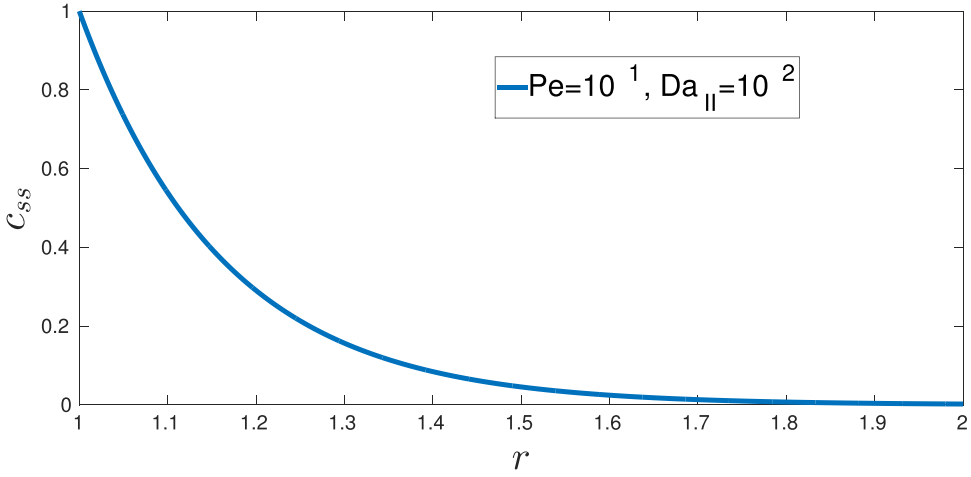

Fig. 3. Steady state concentration profile c_{ss} as function of r (Regime B) for a fixed value of $Pe = 10^1$ and $Da_{II} = 10^2$.

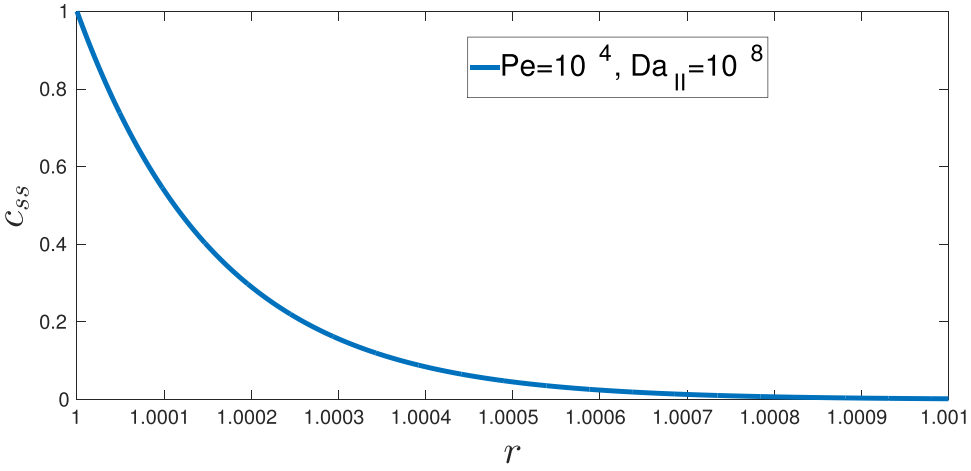

Fig. 4. Steady state concentration profile c_{ss} as function of r (Regime B) for a fixed value of $Pe = 10^4$ and $Da_{II} = 10^8$. The figure seems similar to Fig. 3. Note, however, the different scale on the r-axis compared to Fig. 3.

3.2. *Regime b:* $\mathrm{Da_{II}} \sim \mathrm{Pe}^2$

In regime B we use the following rescaling of the radial coordinate

$$r = 1 + \frac{\bar{r}}{Pe} \Rightarrow \frac{d}{dr} = Pe\frac{d}{d\bar{r}}, \tag{41}$$

to solve equations (35)-(36). We find the following equation for c_{ss} (see Appendix A.2 for a detailed derivation)

$$c_{ss} = \frac{c^\star}{1 - \frac{1}{2}(\sqrt{1+4\beta}-1)} e^{-\frac{1}{2}(\sqrt{1+4\beta}-1)(r-1)Pe}, \quad \beta = \frac{Da_{II}}{Pe^2}. \tag{42}$$

For small values of Da_{II} we observe a non-horizontal profile (see Fig. 3); for larger values of Da_{II} the entire reservoir remains at the initial concentration (see Fig. 4).

3.3. *Regime c* $\mathrm{Da_{II}} \gg \mathrm{Pe}^2$

In Regime C the convection term $\frac{(Pe-1)}{r}\frac{dc_{ss}}{dr}$ can be neglected, as we will show in Appendix A.3. Solving equations ((35)-(36) yields (see Appendix A.3 for a detailed derivation)

$$c_{ss} = \frac{c^\star Pe}{\sqrt{Da_{II}}} e^{-\sqrt{Da_{II}}(r-1)} \tag{43}$$

In this case we observe that the whole reservoir is at the initial concentration. Note that the width of the concentration layer $\sim \frac{1}{\sqrt{Da_{II}}}$; this width may become in the order of the pore length, which means that application of our Darcy scale model is questionable in this part of regime C.

3.4. *Phase space*

In order to discuss the behaviour of $c_{ss}(r)$ we introduce the following two distances: $r_{0.99}$ and $r_{0.01}$ (see Fig. 6).

The distance $r_{0.99}$ is defined as follows: the reservoir is almost at the injection concentration (99% of the injection concentration or higher) until $r = r_{0.99}$. This means that the whole reservoir is (eventually almost) at the injection concentration for large $r = r_{0.99}$.

The distance $r_{0.01}$ is defined in a similar way: the reservoir is almost at the (zero) initial concentration (1% of the injection concentration or lower) after $r = r_{0.01}$. Note that the parameter $r_{0.01}$ is also a measure of the width of the concentration profile, see Fig. 6). This means that the reservoir remains at the initial concentration if this width $r_{0.01} - 1$ is very small, i.e., $r_{0.01} \approx 1$.

The distances $r_{0.99}$ and $r_{0.01}$ allow us to subdivide the full $PeDa_{II}$-parameter space in four regions with distinct physical behaviour.

For some values of (Pe, Da_{II}) the reaction is so slow that the whole reservoir is (eventually) at the injection concentration. We will call this subdomain of the (Pe, Da_{II}) phase space "Region I"

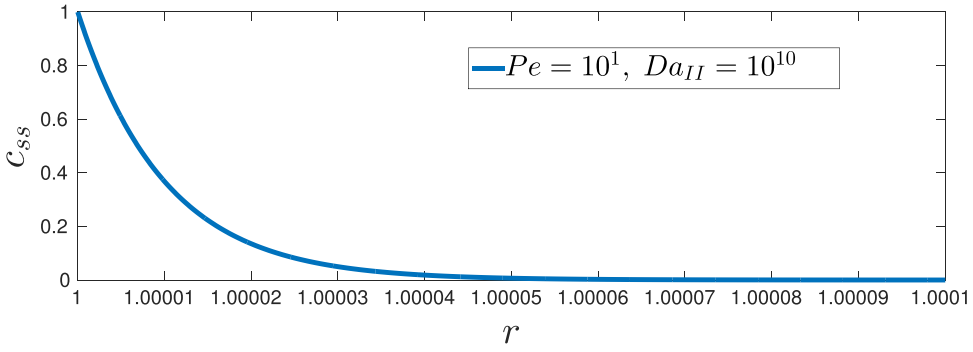

Fig. 5. Steady state concentration profile c_{ss} as function of r (Regime C) for a fixed value of $Pe = 10^1$ and $Da_{II} = 10^{10}$. Note the very fine scale on the r-axis, which runs from 1.0000–1.0001.

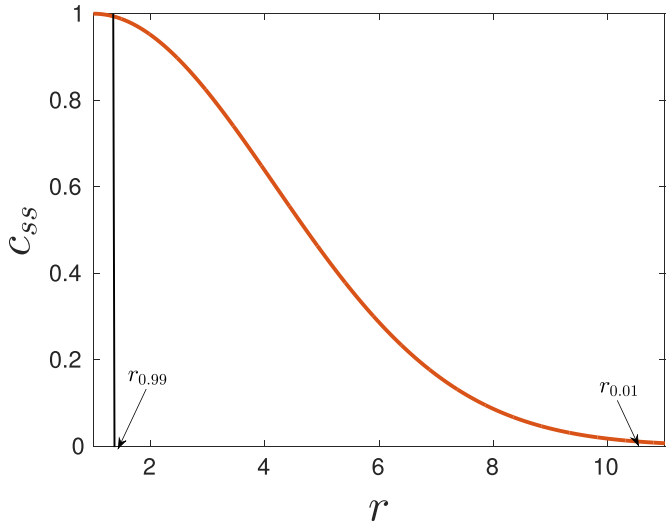

Fig. 6. The concentration profile $c_{ss}(r)$ for $Pe = 10^3$ and $Da_{II} = 10^2$ (Regime B) The equilibrium distances $r_{0.99} = 1.4$ and $r_{0.01} = 10.6$ are shown as well. For $1 \le r \le r_{0.99}$ we have $c_{ss} \approx c_{ss}(1)$; this part of the reservoir is at injection concentration. For $r \ge r_{0.01}$ we have $c_{ss} \approx 0$; this part of the reservoir is at the initial concentration.

("no reaction"). Region I is characterized by high values of $r_{0.99}$; for our figures we will use $r_{0.99} = 100$ as boundary for Region I.

High reaction rates lead to a situation where all reaction takes place at the inlet; almost no reaction takes place in the remainder of the reservoir, which remains at the initial concentration. We will call this subdomain of the (Pe, Da_{II}) phase space "Region III" ("equilibrium"). Region III is characterized by values of $r_{0.01}$ close to one; for our figures we will use $r_{0.01} = 1.01$ as boundary for Region III.

The range of values of Pe and Da_{II} in between Regions I and III in the phasespace is called Region II ("kinetics"). In this part of the phasespace $c_{ss}(r)$ is neither at the initial nor at the injection concentration but varies between these values. In this Region II kinetics has to be taken into account.

Very high reaction rates may lead to a situation where the reaction takes places over distances over the order of a single pore $R_{char} r_{0.01} \sim 10^{-6}$ m. In this case the Darcy-approximation may be questionable. We will call this subdomain of the (Pe, Da_{II}) phase space Region IV ("Darcy-Brinkman").

In summary:

Region I ("no reaction") The reaction rate is so low that the reaction can be neglected. The whole reservoir is eventually at the injection concentration.

Region II ("kinetics") Intermediate reaction rate; kinetics have to be taken into account in the whole reservoir.

Region III ("equilibrium" High reaction rate; all reactions take place very close to the inlet, where the concentration varies from injection to initial concentration. Most of the reservoir remains at the initial concentration.

Region IV ("Darcy-Brinkman") The width of the reaction zone becomes of the order of the poresize, which means that our Darcy-scale equations may not hold anymore.

4. Quantitative behaviour of minerals in three regions of the phase space

By way of example we choose three minerals that are representative for the three regions I, II, ad III. For all regions we introduce t_{eq}, being the time needed to reach the steady state. For regions II and III, we also introduce the equilibrium distance $r_{eq} \approx r_{0.01}$. This equilibrium distance r_{eq} is the distance beyond which the reservoir is (almost) at the initial concentration, see Fig. 6.

For an exact computation of the equilibrium time t_{eq} the transient problem (37)-(39) has to be solved. We will not do so in this paper; instead we estimate t_{eq} using the solution of the velocity profile (32).

$$v = \frac{1}{r} \Rightarrow t = \frac{1}{2} r^2 - \frac{1}{2}, \tag{44}$$

which means that we can associate a dimensionless equilibrium time t_{eq} to an equilibrium distance as follows

$$t_{eq} = \frac{1}{2}(r_{eq}^2 - 1). \tag{45}$$

We will use equation (45) to estimate the equilibrium times in this section.

In regions I-III, we observe the following three types of behaviour

Region I no reaction; the reservoir is (depending on r and t) either at injection or at initial concentration.

Region II $r_{eq} \approx 1$; kinetics have to be taken into account until $t \approx t_{eq}$. However, for $t \gg t_{eq}$ the concentration profile may be approximated by the steady state profile $c_{ss}(r)$.

Region III $r_{eq} \gg 1$; the whole reservoir remains at the initial concentration.

4.1. Discussion of K-Feldspar (regions i and II)

For K-Feldspar we have $Da_{II} = 1.0 \cdot 10^{-7}$ (low sal) or $Da_{II} = 2.0 \cdot 10^{-9}$ (alkaline pH $>$ 7) (see Table 4). Using Fig. 7 (yellow dots)

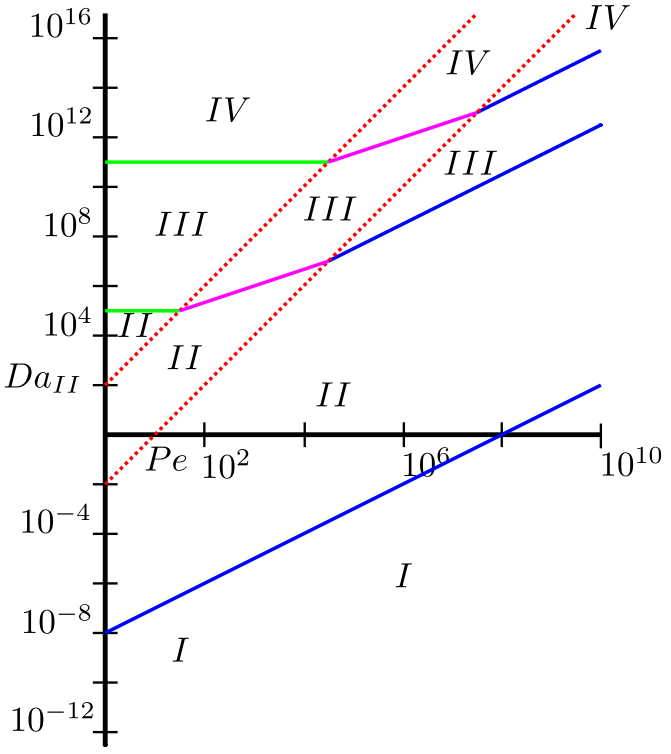

Fig. 7. The full $PeDa_{II}$-phase space is subdivided in four regions, viz., region I (reaction can be neglected), region II (kinetics has to be takes into account), region III (fast convergence to chemical equilibrium) and region IV (application beyond Darcy scale). The red dotted lines only indicate the different mathematical approximations used. (For interpretation of the references to colour in this figure legend, the reader is referred to the web version of this article.)

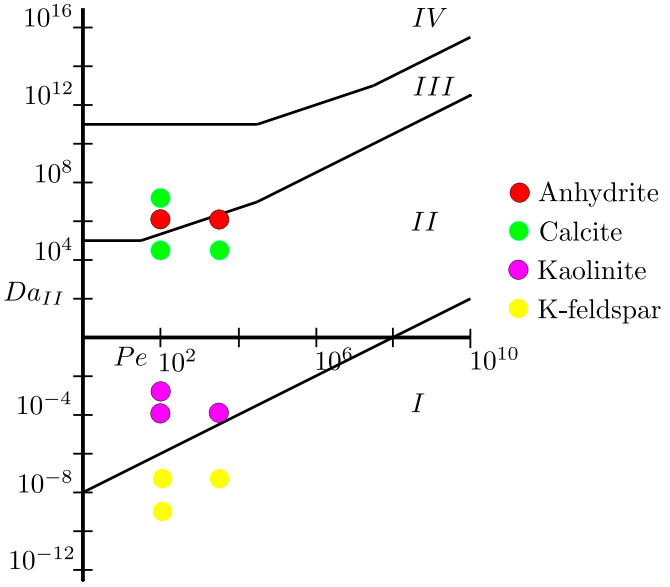

Fig. 8. The position of four different minerals in the $PeDa_{II}$-phasespace under three different conditions. In some cases (K-Feldspar, Kaolinite) the minerals are in the same region for all circumstances investigated, whereas in other cases (Calcite, Anhydrite) the region has to be determined on a case-by-case basis.

we observe that K-Feldspar is (mostly) in Region I in the $PeDa_{II}$-phasespace. This is confirmed by the computation of $r_{0.99}$; using equation (40) we find for $Pe = 10^2$, $Da_{II} = 1.0 \cdot 10^{-7}$

$$c^\star e^{-\alpha(r_{0.99}^2 - 1)} = 0.99 c^\star \Rightarrow r_{0.99} \approx 4.5 \cdot 10^3$$

(for the other two cases $r_{0.99}$ is even bigger). This corresponds to a dimensional distance $R_{0.99} = 450$ m, which is of the order of the size of the reservoir: eventually the whole reservoir is at the injection concentration.

We can approximate the full time dependent concentration profile (using equation (44) by

$$c_{ss}(r,t) = \begin{cases} 0 & t < \frac{1}{2}(r^2 - 1) \\ c^\star & t \geq \frac{1}{2}(r^2 - 1) \end{cases}. \tag{46}$$

This means that at, e.g., $r = 10$ (corresponding to 1 m) the concentration is equal to zero until $t = \frac{99}{2}$ (corresponding to $T = \frac{99}{2} T_c \approx$ 12 days) and equal to $c^\star$ afterwards.

4.2. Discussion of kaolinite (region II)

For Kaolinite we have $Da_{II} = 2.0 \cdot 10^{-3}$ (low sal) or $Da_{II} = 5.0 \cdot 10^{-6}$ (alkaline) (see Table 4). Using Fig. 7 (purple dots) we observe that Kaolinite is in Region II in the $PeDa_{II}$-phasespace. This is confirmed by the computation of $r_{0.99}$; using equation (40)we find for, e.g., $Pe = 10^2$, $Da_{II} = 2.0 \cdot 10^{-3}$,

$$c^\star e^{-\alpha(r_{0.01}^2 - 1)} = 0.01 c^\star \Rightarrow r_{0.01} \approx 6.8 \cdot 10^2.$$

and

$$c^\star e^{-\alpha(r_{0.99}^2 - 1)} = 0.99 c^\star \Rightarrow r_{0.99} \approx 33,$$

which means that kinetics have to be taken into account into a part of the reservoir (between 3.3 and 68 m) until the steady state is reached. The time required to reach the (spatially dependent) equilibrium solution can be estimated using equation (44) by

$$t_{eq} \approx \frac{1}{2}(r_{0.01}^2 - 1) \approx 2.3 \cdot 10^5,$$

which corresponds to $T_{eq} = 2.5 \cdot 10^5$ days. This means that kinetics has to be taken into account.

4.3. Discussion of calcite (boundary regions II and III)

For Calcite we have $Da_{II} = 6.0 \cdot 10^5$ (low sal) or $Da_{II} = 2.0 \cdot 10^8$ (alkaline) (see Table 4). Using Fig. 7 (green dots) we observe that Calcite is either in Region II or in Region III in the $PeDa_{II}$-phasespace. This is confirmed by the computation of $r_{0.01}$; using equation (42) we find for $Pe = 5 \cdot 10^3$, $Da_{II} = 6.0 \cdot 10^5$ that

$$r_{0.01} = 1.04.$$

The time required to reach the (spatially dependent) equilibrium solution can be estimated using equation (44)

$$t_{eq} \approx \frac{1}{2}(r_{0.01}^2 - 1) \approx 0.04$$

which corresponds to $T_{eq} \approx 0.05$ days, i.e., roughly 1 h. This means that for $0 \leq T \leq T_{eq}$ kinetics need to be taken into account. For $T \geq T_{eq}$ the steady state saturation profile (42) may be used.

For the alkaline case we find ($Pe = 10^2$ and $Da_{II} = 2.0 \cdot 10^8$) using equation (43)

$$r_{0.01} = 1.0003,$$

which means that Calcite remains at the initial concentration in this case.

4.4. Discussion of anhydrite (region III)

For Anhydrite we have $Da_{II} = 2.7 \cdot 10^7$ (low sal) or $Da_{II} = 1.0 \cdot 10^7$ (alkaline) (see Table 4). Using Fig. 7(red dots) we observe that Anhydrite is in Region III in the $PeDa_{II}$-phasespace. This is confirmed by the computation of $r_{0.01}$; using equation (43) we find for $Pe = 10^2$, $Da_{II} = 1.0 \cdot 10^7$ that

$$r_{0.01} = 1.001$$

(and smaller for the other cases), which means that Anhydrite remains at the initial concentration in all cases.

5. Conclusion

Reactive flow modeling involves vastly different reaction rates, i.e., differing by many orders of magnitude. Consequently some reactions proceed so slow that in the time frame considered they can be disregarded. Other reactions occur so fast that they are well described by thermodynamic equilibrium in the time and spatial region of interest. Very fast and very slow reactions can be decoupled from the reactions that occur at intermediate rates; at intermediate rates kinetics needs to be taken into account. It is possible to categorize selected reactions as slow, fast or intermediate. We model 2D radially symmetric reactive flow with a reaction-convection-diffusion equation. Using the solution of the steady state profile we subdivide the $PeDa_{II}$ phasespace in three regions. Region I (slow reaction); reaction can be ignored and minerals are convected along with the flow. The minerals are either at the injection or initial concentration, depending on location and time. Region III (fast reaction); all reaction takes places in a very narrow region around the injection point. The reservoir remains at the initial concentration beyond this narrow region. Kinetics can be neglected in (almost) all of the computational domain. Finally, Region II (intermediate reaction); initially kinetics need to be taken into account. Eventually, beyond an equilibrium time a spatially dependent concentration profile is reached; after this equilibrium time, which can be much longer than the time of interest this concentration profile can be used; so in general kinetics has to be taken into account. We show in explicit examples, the location in phase space of a few selected minerals depending on salinity, pH and temperature. The computation of the Pe and Da_{II} numbers for a (any) specific process makes it possible to determine in which of the Regimes I-III a process is, i.e., for which time window kinetics has to be taken into account. We note that the conditions, e.g., pH, salinity and temperature may be essential for assigning the reaction to the correct region in phase space. The methodology described can be applied to any mineral precipitation/decomposition problem and consequently greatly simplifies the model equations.

Appendix A. Mathematical derivations and proofs

A1. Concentration profile in regime a

In Regime A the diffusion term $\frac{d^2c_{ss}}{dr^2}$ can be neglected, as we will show in equations (A.4)-(A.7) below. This means that equation (35) reduces to

$$0 = \frac{(Pe-1)}{r}\frac{dc_{ss}}{dr} + Da_{II}c_{ss}, \tag{A.1}$$

which can be solved using separation of variables; we obtain

$$c_{ss} = Ke^{-\alpha r^2},\ \alpha = \frac{Da_{II}}{2(Pe-1)}, \tag{A.2}$$

where the integration constant K can be determined using the boundary condition (BC) (36). We compute $c_{ss}(1)$ and $\frac{dc_{ss}}{dr}|_{r=1}$

$$c_{ss}(1) = Ke^{-\alpha}\ \frac{dc_{ss}}{dr}|_{r=1} = -2\alpha Ke^{-\alpha}$$

and substitute these expressions in the BC (36) to obtain

$$Ke^{-\alpha}(1 - \frac{-2\alpha}{Pe}) = c^\star.$$

Note that $\frac{2\alpha}{Pe} = \frac{Da_{II}}{Pe(Pe-1)} \ll 1$ which means that this contribution can be neglected; solving for K yields $K = c^\star e^{\alpha}$ which means that we obtain

$$c_{ss} = c^\star e^{-\alpha(r^2-1)},\ \alpha = \frac{Da_{II}}{2(Pe-1)}. \tag{A.3}$$

We will now first show that the diffusion term can indeed be neglected. Using the solution (A.3) we find

$$\frac{dc_{ss}}{dr^2} = K(\alpha^2 r^2 - \alpha)e^{-\alpha r^2}, \tag{A.4}$$

which means that this term can be neglected with respect to the reaction term (or equivalently with respect to the convection term) if

$$Da_{II}c_{ss} = Da_{II}Ke^{-\alpha r^2} \gg K(\alpha^2 r^2 - \alpha)e^{-\alpha r^2}. \tag{A.5}$$

This holds if both $Da_{II} \gg \alpha$ and $Da_{II} \gg \alpha^2$, i.e., if

$$Da_{II} \gg \alpha = \frac{Da_{II}}{2(Pe-1)} \Rightarrow Pe \gg 1, \tag{A.6}$$

which is always satisfied in our regime of interest and if

$$Da_{II} \gg \alpha^2 = \frac{Da_{II}^2}{4(Pe-1)^2} \Rightarrow Da_{II} \ll Pe^2, \tag{A.7}$$

which is satisfied due to our restriction on Regime A.

A2. Concentration profile in regime b

In regime B we use the following rescaling of the radial coordinate

$$r = 1 + \frac{\bar{r}}{Pe} \Rightarrow \frac{d}{dr} = Pe\frac{d}{d\bar{r}}, \tag{A.8}$$

which means that equation (35) becomes

$$Pe^2\frac{d^2c_{ss}}{d\bar{r}^2} = \frac{Pe(Pe-1)}{1+\frac{\bar{r}}{Pe}}\frac{dc_{ss}}{d\bar{r}} + Da_{II}c_{ss}, \tag{A.9}$$

which reduces to

$$\frac{d^2c_{ss}}{d\bar{r}^2} = \frac{dc_{ss}}{d\bar{r}} + \beta c_{ss},\ \beta = \frac{Da_{II}}{Pe^2}, \tag{A.10}$$

because $1 + \frac{\bar{r}}{Pe} \approx 1$ and $Pe(Pe-1) \approx Pe^2$ because Pe is large. Eq. A.10 is a second order linear ode with constant coefficients. The solution of Eq. A.10 is

$$c_{ss}\bar{r} = K_1 e^{-\frac{1}{2}(\sqrt{1+4\beta}-1)\bar{r}} + K_2 e^{\frac{1}{2}(\sqrt{1+4\beta}+1)\bar{r}}. \tag{A.11}$$

Due to the second boundary condition (36) we have $K_2 = 0$ which means that we find

$$c_{ss}(\bar{r}) = K_1 e^{-\frac{1}{2}(\sqrt{1+4\beta}-1)\bar{r}} = K_1 e^{-\frac{1}{2}(\sqrt{1+4\beta}-1)(r-1)Pe}. \tag{A.12}$$

Using the first boundary condition (36) we can determine K_1

$$c_{ss}(1) - \frac{1}{Pe}\frac{dc_{ss}}{dr} = K_1(1 - \frac{1}{2}(\sqrt{1+4\beta}-1)) = c^\star \Rightarrow K_1 = \frac{c^\star}{1-\frac{1}{2}(\sqrt{1+4\beta}-1)} \tag{A.13}$$

and we find

$$c_{ss} = \frac{c^\star}{1-\frac{1}{2}(\sqrt{1+4\beta}-1)} e^{-\frac{1}{2}(\sqrt{1+4\beta}-1)(r-1)Pe} \tag{A.14}$$

A3. Concentration profile in regime c

In Regime C the convection term $\frac{(Pe-1)}{r}\frac{dc_{ss}}{dr}$ can be neglected. This means that equation (35) reduces to

$$\frac{d^2c_{ss}}{dr^2} = Da_{II}c_{ss}, \tag{A.15}$$

which can be solved

$$c_{ss} = K_1 e^{-\sqrt{Da_{II}}r} + K_2 e^{\sqrt{Da_{II}}r}, \tag{A.16}$$

where $K_2 = 0$ due to the second boundary condition (36). The integration constant K_1 can be determined using the first boundary condition (36) as follows

$$c_{ss}(1) - \frac{1}{Pe}\frac{dc_{ss}}{dr}|_{r=1} = K_1(1 + \frac{\sqrt{Da_{II}}}{Pe})e^{-\sqrt{Da_{II}}} = c^\star.$$

Note that $\frac{Da_{II}}{Pe^2} \gg 1$ in Regime C which means that the contribution of $1 + \frac{\sqrt{Da_{II}}}{Pe} \approx \frac{\sqrt{Da_{II}}}{Pe}$; we obtain

$$K_1 = c^\star e^{\sqrt{Da_{II}}}\frac{Pe}{\sqrt{Da_{II}}},$$

and we finally find

$$c_{ss} = \frac{c^\star Pe}{\sqrt{Da_{II}}}e^{-\sqrt{Da_{II}}(r-1)}. \tag{A.17}$$

We will now first show that the convection term indeed can be neglected. Using solution (A.17) we find

$$\frac{dc_{ss}}{dr} = -Pec^\star e^{-\sqrt{Da_{II}}(r-1)}, \tag{A.18}$$

which can be neglected with respect to the reaction term $Da_{II}c_{ss}$ if (or equivalently with respect to the difussion term) if

$$Da_{II}c_{ss} = Pe\sqrt{Da_{II}}c^\star e^{-\sqrt{Da_{II}}(r-1)} \gg Pe(Pe-1)c^\star e^{-\sqrt{Da_{II}}(r-1)}. \tag{A.19}$$

This holds if $\sqrt{Da_{II}} \gg Pe - 1$, i.e., if $Da_{II} \gg Pe^2$, which is indeed satisfied due to our assumption on regime C.

Appendix B. Analysis of the $PeDa_{II}$-phasespace

Using the notion of the distances $r_{0.99}$ and $r_{0.01}$, we can subdivide the (Pe, Da_{II})- phase space in four regions.

The first distance $r = r_{0.99}$ is associated with Region I and is defined as follows

$$c \geq 0.99c^\star \text{ for } 1 \leq r \leq r_{0.99}, \tag{B.1}$$

i.e., the reservoir is at injection concentration until $r_{0.99}$. This means that if $r_{0.99} \approx r_{res}$ the entire reservoir is (eventually) almost at injection concentration. We define our Region I now as follows:

$$\text{Region I} = \{(Pe, Da_{II}) \mid r_{0.99} \geq r_{res}\}, \tag{B.2}$$

where the dimensionless reservoir size $r_{res} = 10^3$ with our choice of scales.

The second distance $r_{0.01}$ is defined similarly

$$c \leq 0.01c^\star \text{ for } r \geq r_{0.01}, \tag{B.3}$$

i.e., the reservoir is at initial concentration beyond $r_{0.01}$. This means that if $r_{0.01} \approx 1$ most of the reservoir is at the initial concentration. We define our Region III now as follows:

$$\text{Region III} = \{(Pe, Da_{II}) \mid 1 + 10^{-5} \leq r_{0.01} \leq 1 + 10^{-2}\}. \tag{B.4}$$

The region in between Region I and Region III is Region II, i.e.,

$$\text{Region II} = \{(Pe, Da_{II}) \mid r_{0.01} > 1 + 10^{-2},\ r_{0.99} < r_{res}\}. \tag{B.5}$$

For very small values of $r_{0.01}$ we have to be careful. If $r_{0.01} < 1 + 10^{-5}$, the dimensionless width of the reactive region equals 10^{-5}, which in full dimensions equals 10^{-6} m with our length scale. This is of the order of the pore size; the validity of our model equations becomes questionable. This leads to the definition of region IV:

$$\text{Region IV} = \{(Pe, Da_{II}) \mid r_{0.01} < 1 + 10^{-5}\}. \tag{B.6}$$

Using the explicit analytical expressions for c_{ss} derived in Section 3 we will subdivide the full $PeDa_{II}$-phase space in each of the three regimes in (up to) four regions in the following subsections.

B1. Regime a

In regime A we have $Da_{II} \ll Pe^2$; for our numerical pictures we will use $Da_{II} \leq 10^{-2}Pe^2$. We will first compute the boundary of Region I. Using the explicit formula (A.3)

$$c_{ss} = c^\star e^{-\alpha(r^2-1)},\ \alpha = \frac{Da_{II}}{2(Pe-1)}$$

and combining the definition of $r_{0.99}$ and the definition of the boundary of Region I as follows

$$c_{ss}(r = r_{0.99} = 10^3) = 0.99c^\star,$$

we can derive a relation between Da_{II} and Pe on the boundary between regions I and II, i.e.,

$$Da_{II} = \frac{-2\ln(0.99)}{10^6 - 1}(Pe - 1) \approx 2 \cdot 10^{-8}Pe.$$

This means that Region I is below the line $Da_{II} = 2 \cdot 10^{-8}Pe$.

A similar computation yields the boundary between Regions II and III, where we have

$$c_{ss}(r = r_{0.01} = 1 + 10^{-2}) = 0.01c^\star,$$

which yields

$$Da_{II} = \frac{-2\ln(0.01)}{(1 + \cdot 10^{-2})^2 - 1}(Pe - 1) \approx 0.5 \cdot 10^3 Pe.$$

We finally compute the boundary between regions III and IV,

$$c_{ss}(r = r_{0.01} = 1 + 10^{-5}) = 0.01c^\star,$$

which yields

$$Da_{II} = \frac{-2\ln(0.01)}{(1 + 10^{-5})^2 - 1}(Pe - 1) \approx 0.5 \cdot 10^6 Pe.$$

Combining these three (blue) boundary lines we obtain the phase space in Fig. B.9. The red line $Da = 10^{-2}Pe^2$ denotes the boundary of Regime A; the equations in this subsection are only valid below the red line.

B2. Regime b

In regime B we have $Da_{II} \sim Pe^2$; for our numerical pictures we will use $10^{-2}Pe^2 < Da_{II} < 10^2Pe^2$. We will first compute the boundary between Regions I and II. Using the explicit formula (A.12) :

$$c_{ss} = K_1 e^{-\frac{1}{2}(\sqrt{Pe^2 + 4Da_{II}} - Pe)(r-1)},$$

we can derive a relation between Da_{II} and Pe, i.e.,

$$\frac{-2\ln(0.99)}{999} = \sqrt{Pe^2 + 4Da_{II}} - Pe,$$

which yields $\frac{Da_{II}}{Pe} < 10^{-6}$ which holds nowhere in Regime B.

A similar computation yields the boundary between Regions II and III,

$$\sqrt{Pe^2 + 4Da_{II}} - Pe = \frac{-2\ln(0.01)}{10^{-2}} = N_l,$$

where the numerical value $N_l \approx 10^3$. This yields the lower purple curve

$$4Da_{II} = N_l^2 + 2N_lPe$$

in Fig. B.10. The boundary between Regions III and IV is found similarly; this boundary is given by the equation

$$4Da_{II} = N_u^2 + 2N_uPe,$$

where $N_u = 10^6$ and is represented by the upper purple curve in Fig. B.10.

The red lines $Da_{II} = 10^{-2}Pe^2$ and $Da_{II} = 10^2Pe^2$ denote the boundary of Regime B; the equations in this subsection are only valid between the red lines. Note that the "Region I" in Regime B is out of our range of interest of (Pe, Da_{II}) values.

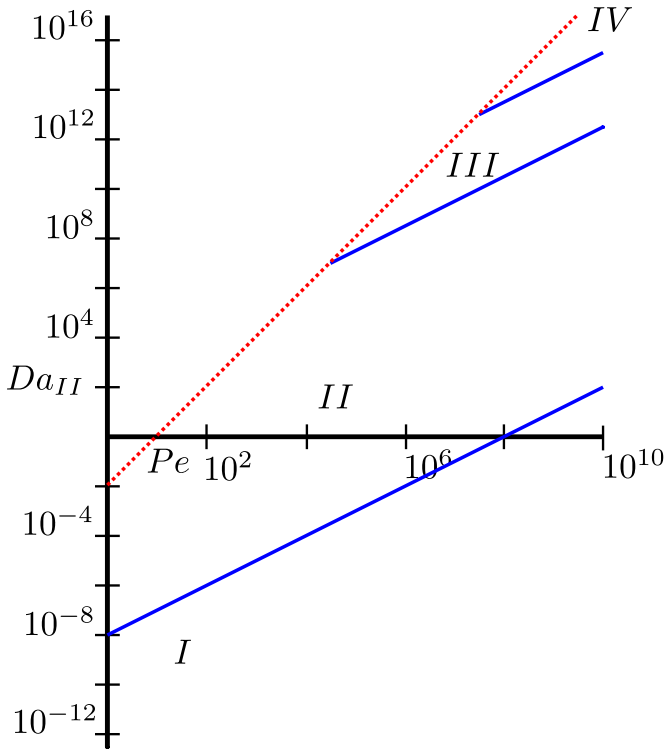

Fig. B.9. The $PeDa_{II}$-phase space in Regime A. The dotted red line denotes the boundary of regime A, i.e., $Da_{II} \leq 10^{-2}Pe^2$. The lowest blue curve denotes the boundary between region I (no reaction) and II (kinetics), the middle blue curve denotes the boundary between region II and region III (equilibrium), and the upper blue curve denotes the boundary between region III and region IV (Darcy-Brinkman). (For interpretation of the references to colour in this figure legend, the reader is referred to the web version of this article.)

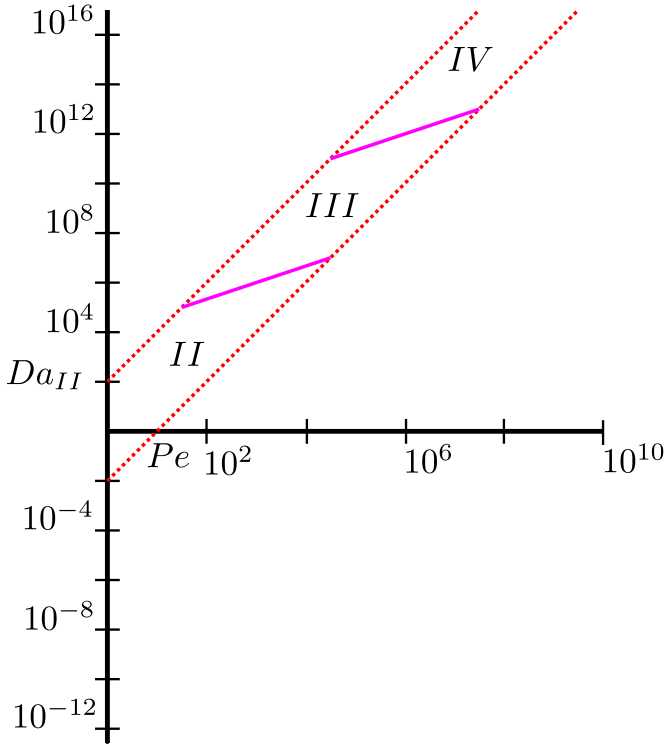

Fig. B.10. The $PeDa_{II}$-phase space in Regime B. The dotted red lines denote the boundaries of regime B, i.e., $10^{-2}Pe^2 \leq Da_{II} \leq 10^{2}Pe^2$. The lower purple curve denotes the boundary between region II (kinetics) and region III (equilibrium), and upper purple curve denotes the boundary between region III and region IV (Darcy-Brinkman). (For interpretation of the references to colour in this figure legend, the reader is referred to the web version of this article.)

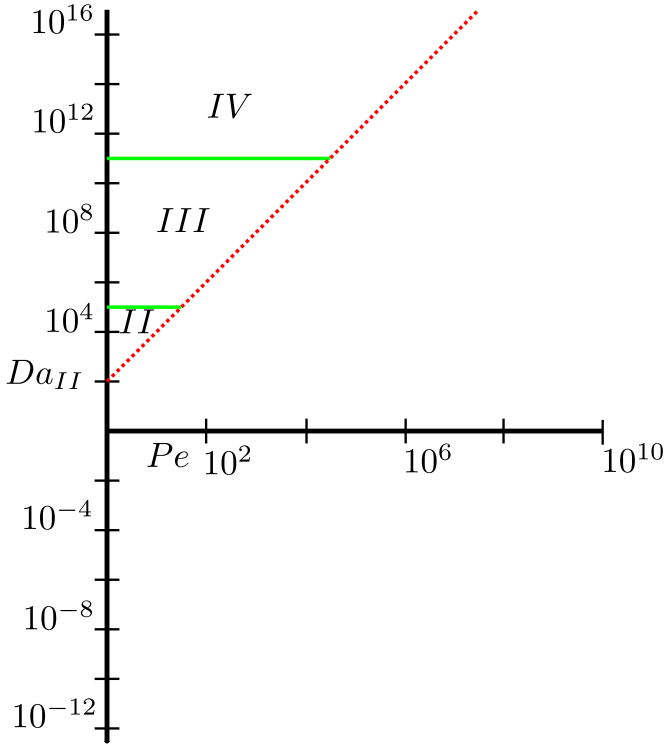

Fig. B.11. The $PeDa_{II}$-phase space in Regime C. The dotted red line denotes the boundary of regime C, i.e., $Da_{II} \geq 10^{2}Pe^2$. The lower green curve denotes the boundary between region II (kinetics) and region III (equilibrium), and upper green curve denotes the boundary between region III and region IV (Darcy-Brinkman). (For interpretation of the references to colour in this figure legend, the reader is referred to the web version of this article.)

B3. Phasespace in regime c

In regime C we have $Da_{II} \gg Pe^2$; for our numerical pictures we will use $Da_{II} > 10^2 Pe^2$. We will use the explicit formula (A.17)

$$c_{ss} = \frac{c^{\star} Pe}{\sqrt{Da_{II}}} e^{-\sqrt{Da_{II}}(r-1)}$$

to compute the boundaries between Regions II and III and between Regions III and IV; the boundary between Regions I and II is out of the range of our interest of (Pe, Da_{II}) values. We observe that the boundaries are at a constant Da_{II} number. For the boundary between Regions II and III we have

$$\ln(0.01) = -\sqrt{Da_{II}} \cdot 10^{-2} \Rightarrow Da_{II} \approx 2 \cdot 10^{5}$$

and for the boundary between Regions III and IV we find similarly

$$\ln(0.01) = -\sqrt{Da_{II}} \cdot 10^{-5} \Rightarrow Da_{II} \approx 2 \cdot 10^{11}.$$

These boundaries are denoted by the green lines in Fig. B.11. Furthermore the red line $Da = 10^2 Pe^2$ denotes the boundary of Regime C. Note that the "Region I" in Regime B is out of the range of our interest of (Pe, Da_{II}) values.

Supplementary material

Supplementary material associated with this article can be found, in the online version, at 10.1016/j.ijheatmasstransfer.2020.119969

References

[1] R. Farajzadeh, T. Matsuura, D. van Batenburg, H.e.a. Dijk, Detailed modeling of the alkali/surfactant/polymer (asp) process by coupling a multipurpose reservoir simulator to the chemistry package phreeqc, SPE Reservoir Evaluation & Engineering 15 (04) (2012) 423–435.

[2] L.W. Lake, R. Johns, B. Rossen, G. Pope, Fundamentals of enhanced oil recovery, Soc. of Pet. Eng., Richardson, Tex, 2014.
[3] H. Farajzadeh R.; Guo, J. van Winden, J. Bruining, Cation exchange in the presence of oil in porous media, ACS Earth & Space Chemistry 1 (2) (2017) 101–112.
[4] H.A. Ohen, F.e.a. Civan, Formation damage in petroleum reservoirs i: modeling, SPE-19380-MS, Society of Petroleum Engineers, 1989.
[5] P. Bedrikovetsky, D. Marchesin, F. Shecaira, A. Souza, P. Milanez, Characterisation of deep bed filtration system from laboratory pressure drop measurements, Petroleum Science and Engineering 32 (2–4) (2001) 167–177.
[6] P. Lichtner, Scaling properties of time-space kinetics mass tranport equations and the local equilibrium limit, Am. J. Sci. 293 (1993) 257–296.
[7] R.B. Knapp, Spatial and temporal scales of local equilibrium in dynamic fluid-rock systems, Geochim. Cosmochim. Acta 53 (8) (1989) 1955–1964.
[8] F. Golfier, C. Zarcone, B. Bazin, R. Lenormand, D. Lasseux, M. QUINTARD, On the ability of a darcy-scale model to capture wormhole formation during the dissolution of a porous medium, J. Fluid Mech. 457 (2002) 213–254.
[9] J.I. Drever, Surface and ground water, weathering, and soils: Treatise on geochemistry, 5, Elsevier, 2005.
[10] C.A.J. Appelo, D. Postma, Geochemistry, groundwater and pollution, CRC press, 2004.
[11] H. Sverdrup, P. Warfvinge, Calculating field weathering rates using a mechanistic geochemical model profile, Appl. Geochem. 8 (3) (1993) 273–283.
[12] H. Sverdrup, P. Warfvinge, Weathering of primary silicate minerals in the natural soil environment in relation to a chemical weathering model, Water Air Soil Pollut. 38 (3–4) (1988) 387–408.
[13] S.A.-M.A. Lake L.W.; Bryant, Geochemistry and fluid flow, Gulf Professional Publishing, 2002.
[14] Y. Al-Khulaifi, Q. Lin, M.J. Blunt, B. Bijeljic, Reservoir-condition pore-scale imaging of dolomite reaction with supercritical co2 acidified brine: effect of pore-structure on reaction rate using velocity distribution analysis, Int. J. Greenhouse Gas Control 68 (2018) 99–111.
[15] Y. Al-Khulaifi, Q. Lin, M.J. Blunt, B. Bijeljic, Pore-scale dissolution by co2 saturated brine in a multimineral carbonate at reservoir conditions: impact of physical and chemical heterogeneity, Water Resour. Res. 55 (4) (2019) 3171–3193.
[16] H. Erfani, V. Joekar-Niasar, R. Farajzadeh, Impact of microheterogeneity on upscaling reactive transport in geothermal energy, ACS Earth and Space Chemistry 3 (9) (2019) 2045–2057.
[17] W.F. Ramirez, A.C. Oen, J.F. Strobel, J.L. Falconer, H.E. Evans, Surface composition of berea sandstone, SPE Form. Eval. 2 (1986) 23–30.
[18] W.J. Moore, Basic physical chemistry, Prentice Hall, 1983.
[19] M. Kazempour, E. Sundstrom, V. Alvarado, Geochemical modeling and experimental evaluation of high-ph floods: impact of water–rock interactions in sandstone, Fuel 92 (1) (2012) 216–230.